

Simple Fabrication of Nickel Sulfide Nanostructured Electrode Using Alternate Dip-Coating Method and Its Supercapacitive Properties

Jinhyeon Kang, Ilhwan Ryu, Geunpyo Choe, Green Kim, Sanggyu Yim*

Department of Chemistry, Kookmin University, Seoul 136-702, South Korea

*E-mail: sgyim@kookmin.ac.kr

Received: 21 June 2017 / Accepted: 4 August 2017 / Published: 12 September 2017

In order to make best use of the superior electrochemical properties of nickel sulfide (NiS) as an electrode material for supercapacitors, increase in surface area through electrode nanostructuring is one of the major issues. However, currently used NiS nanostructuring methods, such as hydrothermal and solvothermal techniques, require high-temperature, long and complicated nano-processes, and hence are not suitable for practical use. In this work, we developed a new, simple method for fabricating porous, nanostructured NiS electrodes by dipping a titanium oxide (TiO₂) nanoparticle-deposited substrate in nickel acetate and sodium sulfide solutions, alternately, at room temperature. One cycle of this alternate dip-coating process takes only 6 min and the amount of deposited NiS can be easily controlled by the number of deposition cycles. Maximum specific capacitance (C_{sp}) of 1044 F/g, comparable to the values of previously reported NiS nanostructure electrodes, was obtained. The voltammetric response retention at high scan rates was also improved by the nanostructuring, exhibiting a value 1.5 times larger than that of the planar film electrode.

Keywords: supercapacitor, nickel sulfide, nanostructured electrode, alternate dip-coating.

1. INTRODUCTION

Supercapacitors have been widely studied as next-generation energy storage devices due to their unique electrochemical properties such as rapid charge-discharge rate, large specific capacitance (C_{sp}) and high power density [1-3]. Especially, pseudocapacitors that utilize fast faradic processes have recently attracted growing interest because they employ higher capacitive properties compared to currently used electrochemical double layer capacitors (EDLCs) [1,4]. Typical electrode materials for pseudocapacitors are transition metal oxides (TMOs) and conductive polymers [5]. Recently, however, transition metal sulfides (TMSs) are emerging as a promising candidate for the electrode material because of their superior properties compared to their corresponding TMOs, such as higher electrical

conductivity, mechanical and thermal stability, and richer redox reactions [6]. Among various TMSs, nickel sulfides (NiS_x) have been most widely investigated owing to their large theoretical capacitance, high electrical conductivity, environmentally friendly characteristics and low price [7-11]. The electrochemical performance of NiS_x in pseudocapacitors involves the reversible reaction between the Ni(II) and Ni(III) oxidation states in the presence of hydroxide anions as follows [12,13]:



However, agglomeration and pulverization of nickel sulfides commonly occur during repetitive charge-discharge processes, which deteriorates the electrochemical properties of the electrodes and hampers their practical applications [7,14]. To solve these problems, two feasible approaches have generally been used: nanostructuring the electrodes [8,15-20] and fabricating composites with carbon-based nanomaterials [11,14,21-23].

Nanostructuring the electrodes is important to improve the capacitive performance of the supercapacitors because the increased surface area can provide increased sites for charge storage processes and an effective path for ion transport [6,24]. In this context, various NiS nanostructures such as nanoparticles [15], nanoflakes [16], nanowires [20], flower-like micro/nano-structures [8], and hollow nanospheres [17] have been proposed. The other approach is fabricating composites with carbon-based nano-materials such as carbon nanotube (CNT) [11,22] and reduced graphene oxide (rGO) [14,21]. However, these approaches require harsh reaction conditions such as hydrothermal or solvothermal processes in an autoclave at significantly high temperatures for a long time, which severely hampers the practical application of the nanostructured NiS electrodes. In addition, most carbon-based nanocomposites have to blend with polymeric binders for prevention of detachment from current collectors, which inhibits ion transport between the electrolytes and active materials [25,26].

To overcome these problems, we developed a much simpler technique, namely alternate dip-coating technique, for facile fabrication of nanostructured NiS electrodes. The technique involves dip-coating of NiS thin films on TiO_2 nanoparticles, alternately, in Ni- and S-precursor solutions at room temperature. One cycle of NiS coating takes only 6 min, and the thickness of the coated films can be easily controlled by the number of coating cycles. TiO_2 nanoparticles were selected as support material due to their high surface area and stability, low cost, and high electrical conductivity ($10^{-5} - 10^{-2}$ S/cm) [27-29]. The fabricated NiS electrodes in this work exhibited a C_{sp} value of 1044 F/g, comparable to the values previously reported for NiS nanostructure electrodes.

2. EXPERIMENTAL

2.1. Fabrication of NiS-coated TiO_2 nanoparticles

A fluorine-doped tin oxide (FTO)-coated glass substrate was subjected to UV- O_3 cleaning for 5 min. A 200 nm-thick porous TiO_2 (p- TiO_2) layer was formed on the cleaned substrate by spin-coating of commercial TiO_2 nanoparticle (NPs) paste (90-T, Dyesol) diluted in ethanol (1:6 weight ratio) at 2500 rpm, followed by annealing at 300°C for 1 h. For the alternate dip-coating of NiS on the TiO_2 layers, 0.15 M Ni- and 0.15 M S-precursor solutions were prepared by dissolving nickel acetate ($\text{Ni}(\text{Ac})_2$, 99%, Aldrich) and sodium sulfide (Na_2S , 98.0%, Aldrich) in a methanol/water (1:1 volume

ratio) mixed solvent, respectively. The TiO₂-deposited FTO substrate was placed in the Ni-precursor solution for 3 min, taken out and blown with N₂ gas, placed in the S-precursor solution for 3 min, and washed with distilled water. This alternate dip-coating cycle was repeated until the desired NiS deposits were obtained. Finally, the NiS-coated TiO₂ electrodes were annealed at 300°C for 1 h. The weights of the NiS deposits were determined by a quartz crystal microbalance (QCM, Stanford Research System QCM 2000). In order to estimate the effect of the porous nanostructure, a compact TiO₂ (c-TiO₂) layer was also prepared for the fabrication of planar thin-film NiS electrode. The c-TiO₂ layer was formed on the substrate via spin-coating of 0.15 M titanium diisopropoxide (TDIP, Sigma-Aldrich) in IPA at 2000 rpm and subsequent annealing at 300°C for 1 h. NiS deposition on the c-TiO₂ layer was then performed using the same alternate dip-coating process.

2.2. Fabrication of asymmetric supercapacitors based on AC//NiS electrodes

The p-TiO₂/NiS and activated carbon (AC) electrodes were employed as positive and negative electrode, respectively, for an asymmetric two-electrode supercapacitor. The slurry for the negative electrode consisting of AC as active material, super-P as conductive additive, and poly(vinylidene difluoride) (PVDF, Aldrich) as polymeric binder (8:1:1 weight ratio) was blade-coated on an FTO-coated glass substrate. The electrode was dried at 90°C for 1 day. The two electrodes were assembled into a sandwich structure with a separator in between, and 2.0 M KOH aqueous solution was used as an electrolyte.

2.3 Characterization

The crystalline structures and morphologies of the TiO₂ and NiS layers were characterized by x-ray diffraction (XRD, Philips PW1827) and field emission scanning electron microscope (FE-SEM, JEOL JSM-7410F, JEOL Ltd.), respectively. The electrochemical properties of the NiS electrodes were evaluated by cyclic voltammetry (CV) and galvanostatic charge-discharge (GCD) technique in 2.0 M aqueous KOH solution at room temperature using a cyclic voltammeter (ZIVE SP2, WonATech). The measurements were performed in a three-electrode electrochemical cell in which the TiO₂/NiS electrode was used as a working electrode, a platinum plate was used as a counter electrode, and Ag/AgCl (in 3.0 M KCl) was used as a reference electrode.

3. RESULTS AND DISCUSSION

The basic strategy for the alternate dip-coating of NiS onto the p-TiO₂ layer is illustrated in Fig. 1. First, the rutile p-TiO₂ layer was prepared by spin-coating of TiO₂ nanoparticles with an average diameter of 20 nm and subsequent annealing at 300°C for 1 h. The crystalline structure of the p-TiO₂ layer was consistent with the reported rutile phase (Fig. 2a). It is known that, among the three representative TiO₂ phases, *i.e.* anatase, brookite and rutile, the rutile phase exhibits the highest electrical conductivity and largest surface area [30,31].

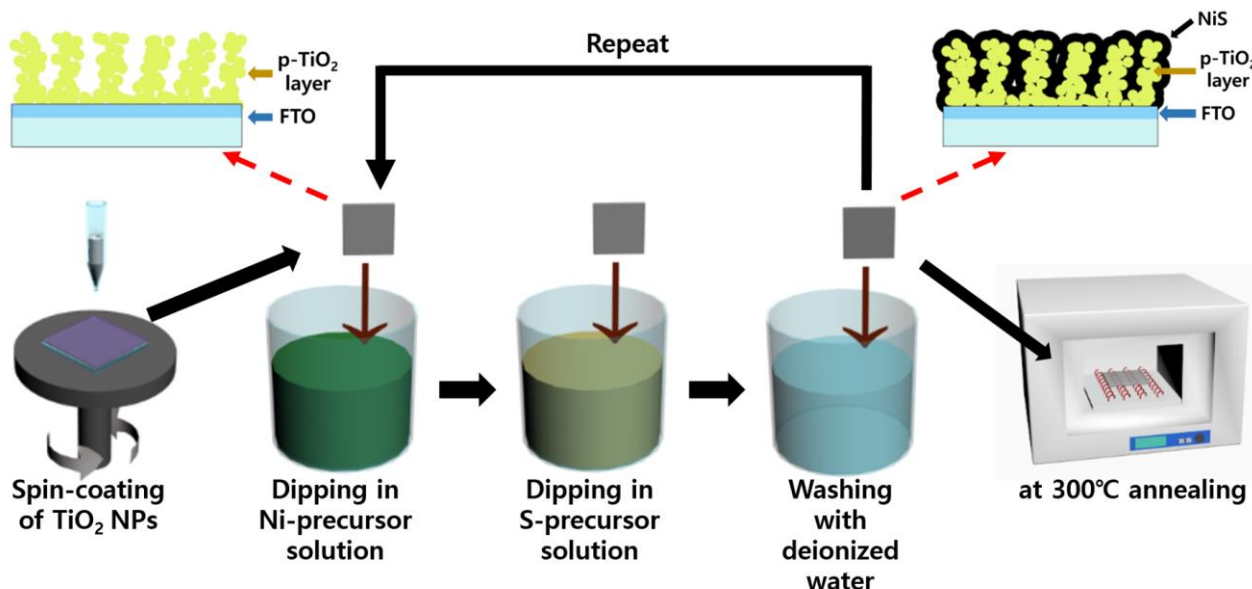


Figure 1. Schematic of the fabrication of nanostructured p-TiO₂/NiS electrodes using the alternate dip-coating process.

The NiS thin films were then formed on this p-TiO₂ layer by alternate dip-coatings in the Ni(Ac)₂ and Na₂S solutions for 3 min each. After the deposition cycles, the p-TiO₂/NiS electrode was annealed at 300°C for 1 h. From the XRD pattern as shown in Fig. 2(b), we can observe that the NiS film is mainly composed of α-phase crystallites; among various phases of NiS crystals, the α-phase crystallites were reported to show the best electrochemical performance as supercapacitor electrode [32]. This new fabrication technique for a nanostructured NiS electrode has a lot of advantages compared to the previously proposed techniques summarized in Table 1. Almost all NiS nanostructures and nanocomposites reported were fabricated using hydrothermal or solvothermal techniques as shown in the table. The reactions were performed in an autoclave at temperatures of 120 – 180°C for 6 – 48 h. However, our process is considerably shorter and simpler, and can be performed at room temperature.

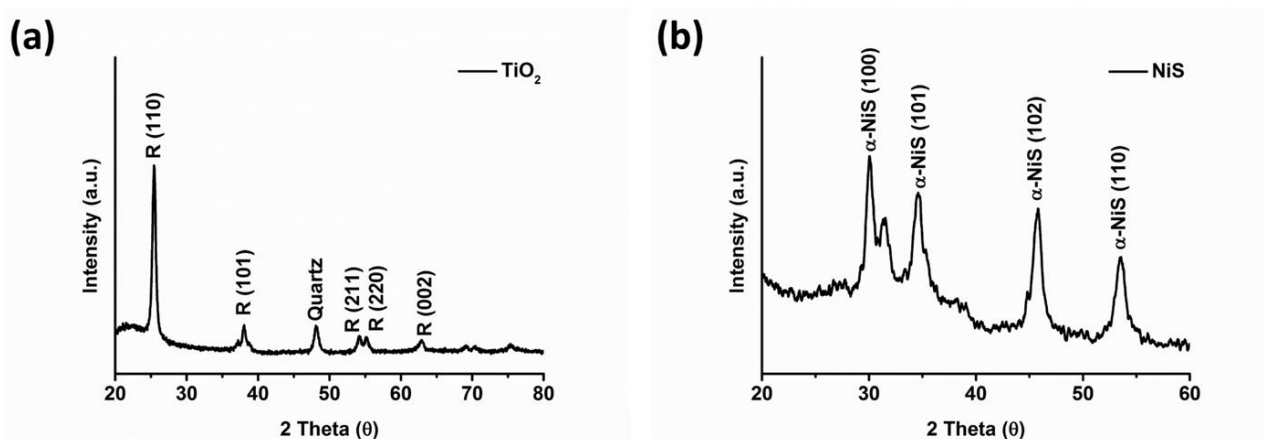
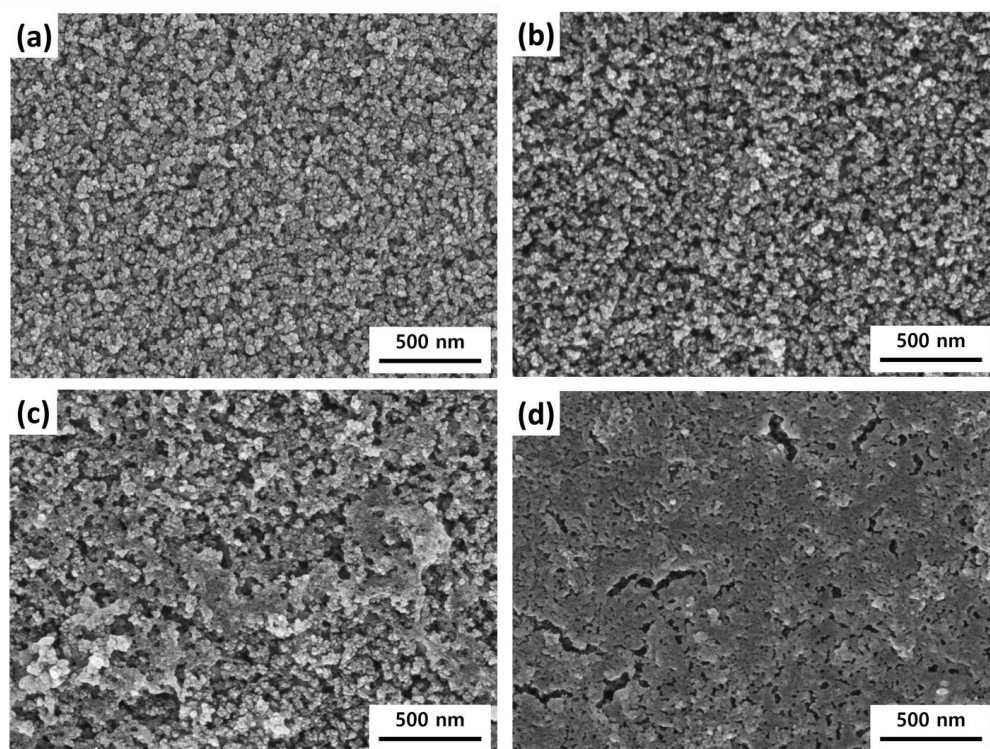


Figure 2. Powder x-ray diffraction patterns of fabricated (a) TiO₂ nanoparticles and (b) NiS films. The diffraction peaks indexed are consistent with standard data from JCPDS.

Table 1. Recently reported results on nanostructured NiS electrodes for supercapacitors.

Structure	Preparation method	Preparation conditions	Capacitance	Ref
Nanoparticle	Solvothermal	120°C, 9-30 h	800 F/g at 0.5 A/g	[15]
Hierarchical flower-like	Solvothermal	150°C, 24 h & 120°C, 24 h	1123 F/g at 1 A/g	[8]
Porous nanoflake	CBD	350°C, 1.5 h & 90°C, 9 h	713 F/g at 2 A/g	[16]
Hollow sphere	Hydrothermal	180°C, 24 h	1848 F/g 1A/g	[17]
Hierarchical porous	Electrodeposition + sulfurization	400°C, 1 h	45 mF/cm ² at 10 mV/s	[18]
Hollow cube	Hydrothermal	120°C, 6 h	875 F/g at 1 A/g	[19]
Nanowire	Hydrothermal	180°C, 9 h	2188 F/g at 3mV/s	[20]
NiS/rGO	Hydrothermal	180°C, 12 h & 160°C, 12 h	905 F/g at 0.5 A/g	[14]
NiS/SWCNT	Solvothermal	180°C, 12 h	1110 F/g at 5 A/g	[11]
NiS/rGO	Solvothermal	180°C, 12 h	852 F/g at 2 A/g	[21]
NiS/Gr/CNT	Solvothermal	180°C, 24 h	2377 F/g at 2mV/s	[22]
NiS/C-aerogel	Solvothermal	180°C, 12 h	1606 F/g at 1 A/g	[23]
NiS/p-TiO ₂ NPs	Alternate dip-coating	RT, 1 h	1044 F/g at 1 mA/cm ²	This work

**Figure 3.** Surface FE-SEM images of the p-TiO₂/NiS electrodes after (a) 0, (b) 1, (c) 7 and (d) 11 cycles of NiS alternate dip-coating process on the p-TiO₂ layer.

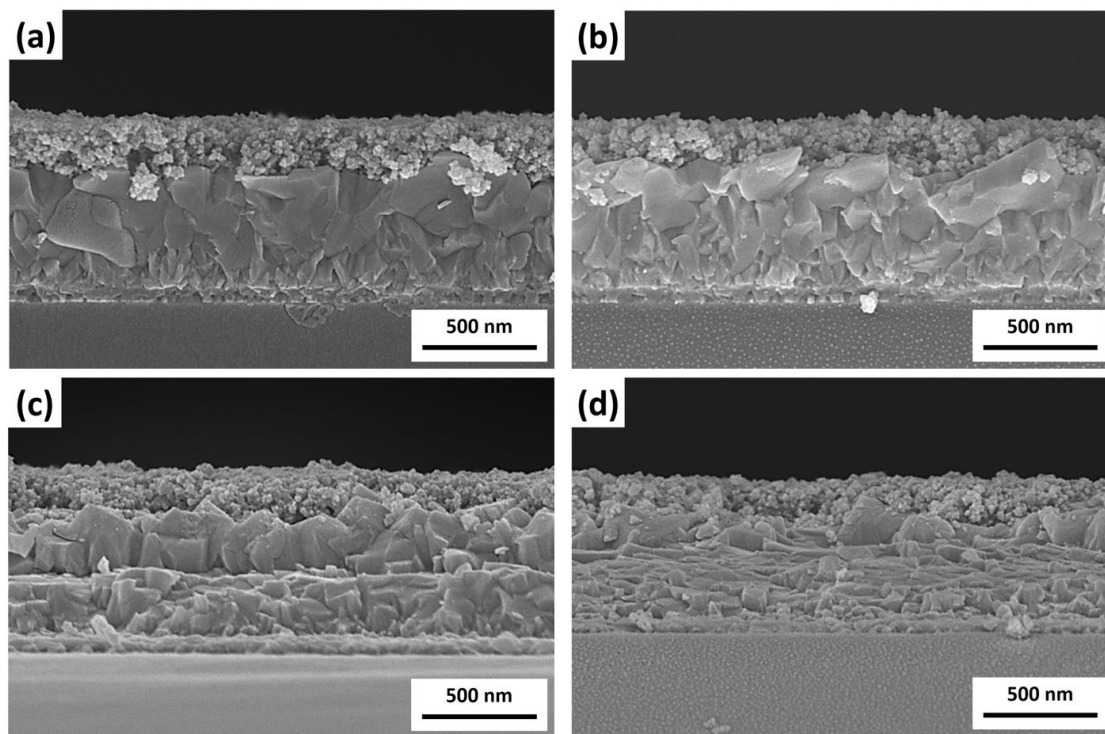


Figure 4. Cross-sectional FE-SEM images of the p-TiO₂/NiS electrodes after (a) 0, (b) 1, (c) 7 and (d) 11 cycles of NiS alternate dip-coating process on the p-TiO₂ layer

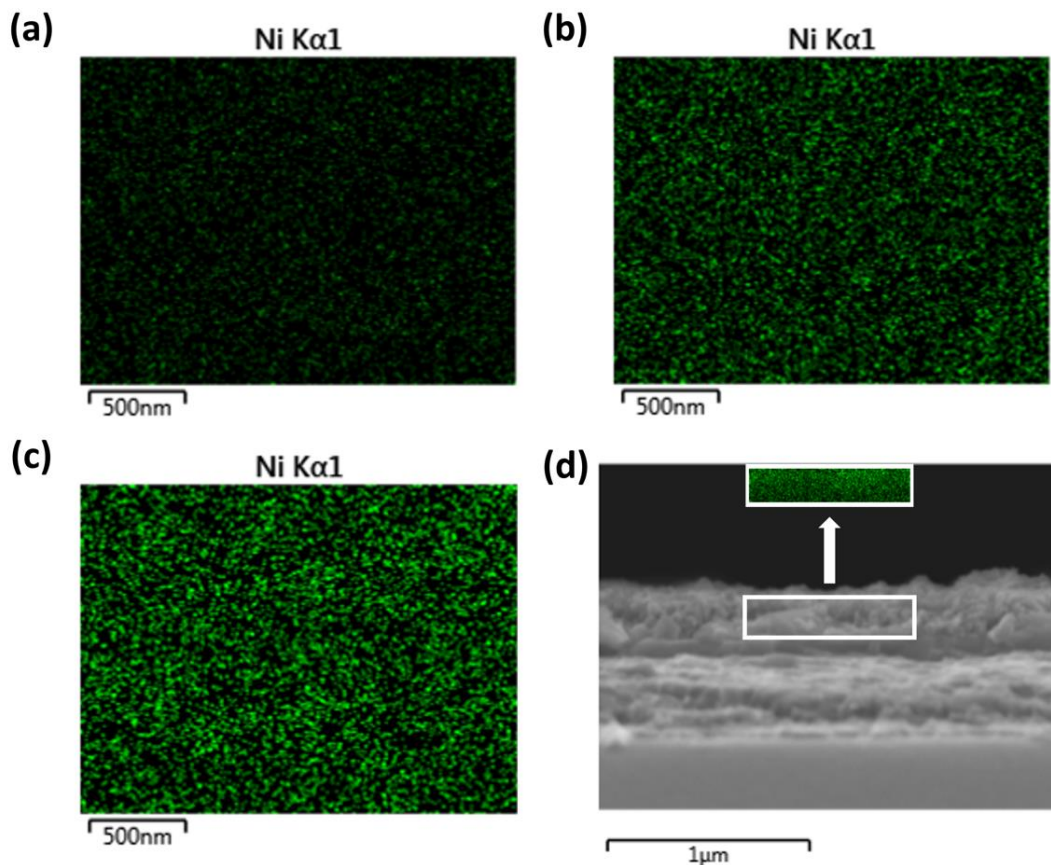


Figure 5. Surface SEM-mapping images for Ni atoms taken after (a) 1, (b) 7 and (c) 11 cycles of NiS alternate dip-coating process on the p-TiO₂ layer. (d) Cross-sectional SEM and SEM-mapping images of (c).

Representative surface FE-SEM images after various alternate dip-coating cycles of NiS on the p-TiO₂ layer are shown in Fig. 3. TiO₂ nanoparticles with diameter of ~20 nm were clearly observed before the deposition of NiS (Fig. 3a). As the number of deposition cycles increased, the size of the nanoparticles gradually increased and some particles were interconnected by the deposited NiS. After 11 alternate dip-coating cycles, almost the entire surface was covered with NiS as shown in Fig. 3(d). The cross-sectional FE-SEM images (Fig. 4) show that the thickness of the p-TiO₂/NiS layer barely changed during the NiS deposition process, indicating that NiS successfully infiltrated into the interstitial spaces of the p-TiO₂ layer during the deposition process, at least up to 11 alternate dip-coating cycles. The elemental mapping results for Ni atoms (Fig. 5) also show that the amount of NiS deposits gradually increased, and the NiS was deposited successfully even on the TiO₂ nanoparticles existing at the bottom of the p-TiO₂ layer.

The NiS deposit weights, measured by QCM, are nearly proportional to the number of deposition cycles, as shown in Fig 6(a). The average deposit weight of NiS was estimated to be 3.4 μg/cm² per alternate dip-coating cycle. The CV measurements for half-cell supercapacitors with the p-TiO₂/NiS electrodes, given various numbers of alternate dip-coating cycles, were performed in a 2.0 M KOH aqueous solution at a potential range from 0.0 V to 0.5 V, as shown in Fig. 6(b). The scan rate for all the measurements was fixed at 10 mV/s. The oxidation and corresponding reduction peaks are located at 0.33 V and 0.24V, respectively. Constant current galvanostatic charge-discharge measurements were also performed; the discharge curves at various current densities within the potential range of 0 – 0.5 V are shown in Fig. 6(c). The potential plateaus at around 0.2 V correspond to the cathodic process revealed in the CV measurements. The specific capacitances are calculated according to the following equation:

$$C_{sp} = \frac{I \cdot \Delta t}{m \cdot \Delta V} \quad (2)$$

where I (A) is the discharge current, m (g) is the mass of deposited NiS, Δt (s) is the total discharge time, and ΔV (V) is the potential drop during the discharge. Fig. 6(d) shows the dependency of the C_{sp} values on the loading amount of NiS. Up to seven alternate dip-coating cycles, the C_{sp} value increased gradually and reached 1044 F/g. However, further deposition of NiS led to a decrease in the C_{sp} value, which was 775 F/g after 11 coating cycles. The drop in specific capacitance is probably the result of over-deposited NiS particles coalescing and gradually blocking electrolyte accessibility to the space in the layer. The obtained maximum C_{sp} value of 1044 F/g is comparable to values previously reported for nanostructured NiS electrodes. As shown in Table I, the reported specific capacitances of the nanostructured NiS electrodes were 800 – 1848 F/g, excluding the values obtained at extraordinarily slow scan rates. Furthermore, the preparation is extremely simple and can be performed at room temperature. The preparation was performed within 2 h, which is significantly shorter than the 6 – 48 h required for conventional hydrothermal or solvothermal techniques. The excellent specific capacitance of the fabricated NiS electrode is reasonably attributed to the porous nanostructured current collector (p-TiO₂) layer with desirable thickness of NiS, which not only facilitates charge transfer but also reduces average distance for ion transportation during the charge-discharge process [33,34].

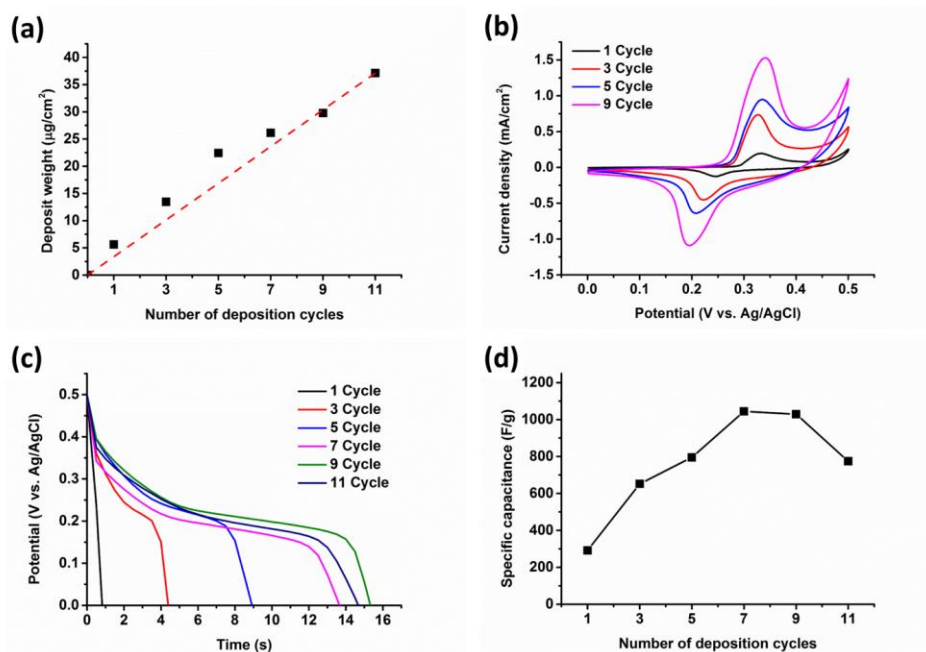


Figure 6. (a) Deposit weights of NiS as a function of the number of alternate dip-coating cycles. (b) Cyclic voltammograms and (c) galvanostatic discharge curves of the p-TiO₂/NiS electrode given various numbers of NiS deposition cycles. The scan rate in (b) and current density in (c) are fixed at 10 mV/s and 1 mA/cm², respectively. (d) Plots of the specific capacitances of the p-TiO₂/NiS electrode as a function of the number of NiS deposition cycles.

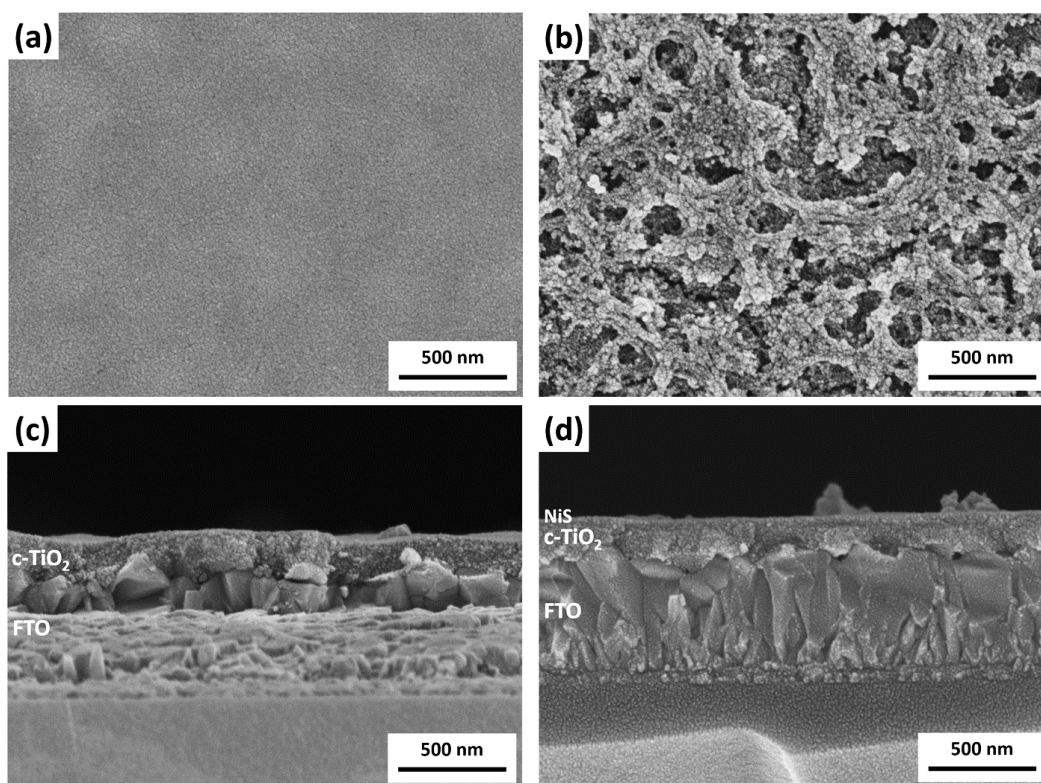


Figure 7. Surface FE-SEM images of the (a) c-TiO₂ layer and (b) c-TiO₂/NiS electrode after 7 cycles of NiS alternate dip-coating process on the c-TiO₂ layer. FE-SEM images of (c) and (d) are cross-sectional ones of (a) and (b), respectively.

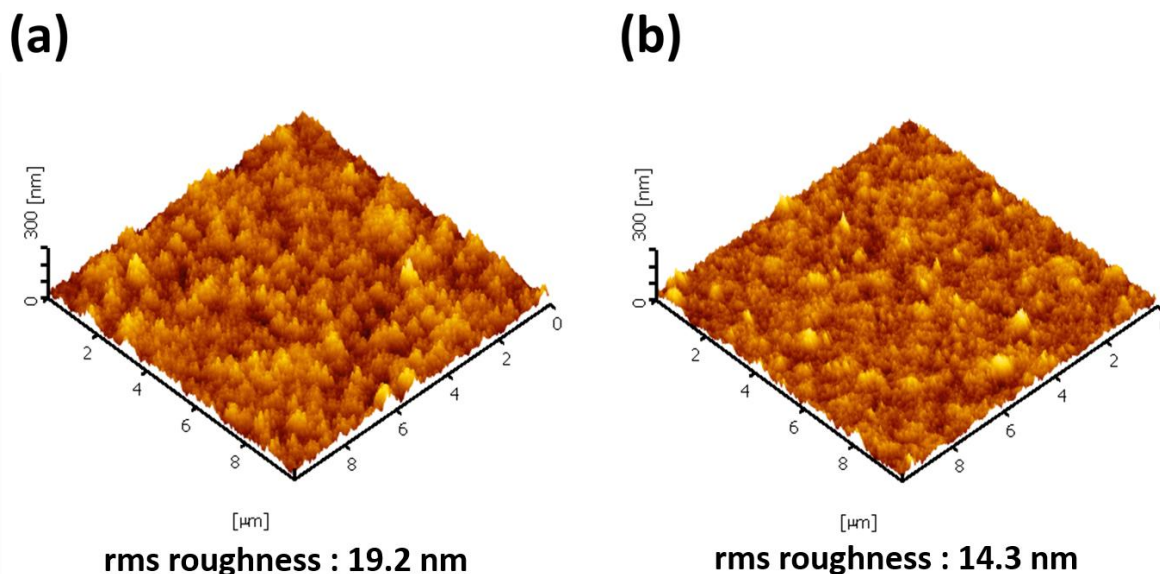


Figure 8. Surface AFM images of the (a) p-TiO₂ and (b) c-TiO₂ layers.

In order to evaluate the effect of the nanostructure, NiS thin films were also fabricated on the compact TiO₂ (c-TiO₂) layer using the same alternate dip-coating cycles and compared. The surface FE-SEM image (Fig. 7a) shows that the surface morphology of this c-TiO₂ layer is significantly smoother than that of the p-TiO₂ layer (Fig. 3a). The AFM measurements also confirm a smaller rms roughness of 14.3 nm for the c-TiO₂ layer compared to that of the p-TiO₂ layer, 19.2 nm, as shown in Fig. 8. The entire surface coverage by NiS deposition on the c-TiO₂ layer was therefore performed more rapidly. Fig. 7(b) shows the surface of the c-TiO₂/NiS electrode after 7 cycles of alternate dip-coating; this surface is similar to the p-TiO₂/NiS electrode surface after 11 cycles. Less infiltration of NiS due to the compact morphology of the c-TiO₂ layer was also observed by cross-sectional FE-SEM measurements. Whereas the thickness of the TiO₂/NiS layer barely changed even after 11 cycles of NiS deposition for the p-TiO₂/NiS electrode (Fig. 4), an increase of the thickness was clearly observed for the c-TiO₂/NiS electrode after 7 cycles of NiS deposition (Fig. 7d). Fig. 9(a) shows the CV curves for the p-TiO₂/NiS and c-TiO₂/NiS electrodes after 7 alternate NiS dip-coating cycles. As expected, the area of the CV contour for the p-TiO₂/NiS electrode is significantly larger than that of c-TiO₂/NiS layer, indicating the superior areal capacitance of the nanostructured electrode. The areal capacitance was calculated by the following equation;

$$C_{\text{areal}} = \frac{\int JdV}{\Delta V(dV/dt)} \quad (3)$$

where J (mA/cm²) is the current density in the CV curve, ΔV (V) is the potential window, and dV/dt (mV/s) is the scan rate. Another merit of electrode nanostructuring is an enhancement in the voltammetric response. Figs. 9(b) and 9(c) show CV curves for the p-TiO₂/NiS and c-TiO₂/NiS electrodes, respectively, at various scan rates ranging from 10 mV/s to 100 mV/s. Oxidation and reduction peaks for both electrodes were observed at 0.33 V and 0.24 V, respectively, at a scan rate of 10 mV/s. As the scan rate increased, the oxidation peak shifted to a more positive potential, and the

reduction peak shifted to a more negative potential; this is due to the increased polarization at high scan rate [35,36]. Fig. 9(d) shows the plots of areal capacitance retention as a function of scan rate. In the case of the c-TiO₂/NiS electrode, the specific capacitance of 5.58 mF/cm² at a scan rate of 10 mV/s dropped to 1.93 mF/cm² at 100 mV/s, and hence the retention was 34.5 %. In contrast, for the p-TiO₂/NiS electrode, the specific capacitance was 30.7 mF/cm² at a scan rate of 10 mV/s; this value decreased to 16.3 mF/cm² at 100 mV/s, and the retention was 53.1 %. This enhancement in voltammetric response of the nanostructured electrode can also be attributed to the efficient access of ions to active sites of the electrode surface. It is well known that the voltammetric current for pseudocapacitive materials originates from surface capacitive reaction and bulk diffusion [26,37,38]; an anodic peak current (i_p) at 25°C can be expressed by the Sevcik equation [39,40]:

$$i_p = 2.69 \times 10^5 \times n^{3/2} \times A \times D^{1/2} \times C_0 \times v^{1/2} \quad (4)$$

where n is the number of electrons involved in the reaction, A is the surface area of the electrode, D is the diffusion coefficient of the electrode material, C_0 is the proton concentration, and v is the scan rate.

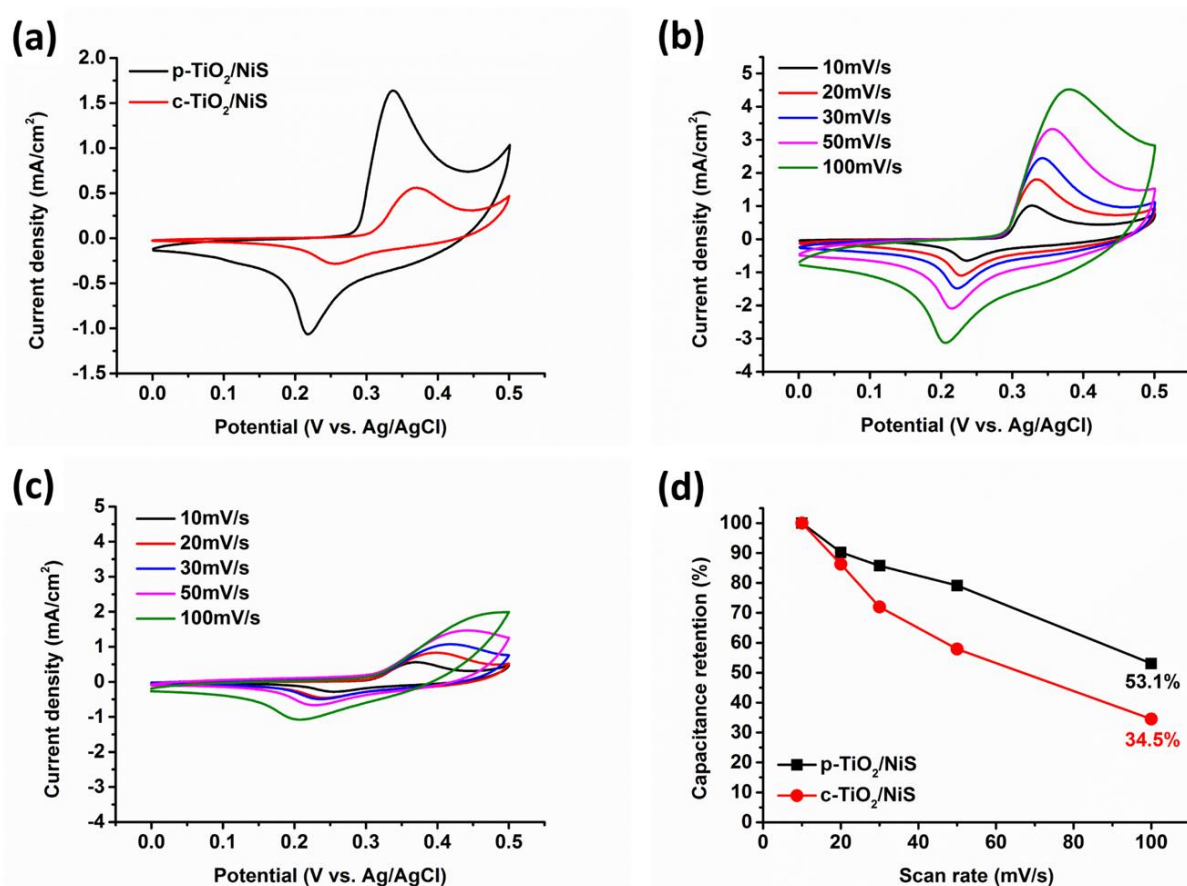


Figure 9. (a) Cyclic voltammograms of the p-TiO₂/NiS (black) and c-TiO₂/NiS (red) electrodes. The number of NiS deposition cycles is 7 and the scan rate is 10 mV/s for both samples. Cyclic voltammograms of the 7-cycle NiS deposited (b) p-TiO₂/NiS and (c) c-TiO₂/NiS electrodes at various scan rates. (d) Plots of the C_{sp} retention for the p-TiO₂/NiS (black) and c-TiO₂/NiS (red) electrodes as a function of the scan rate.

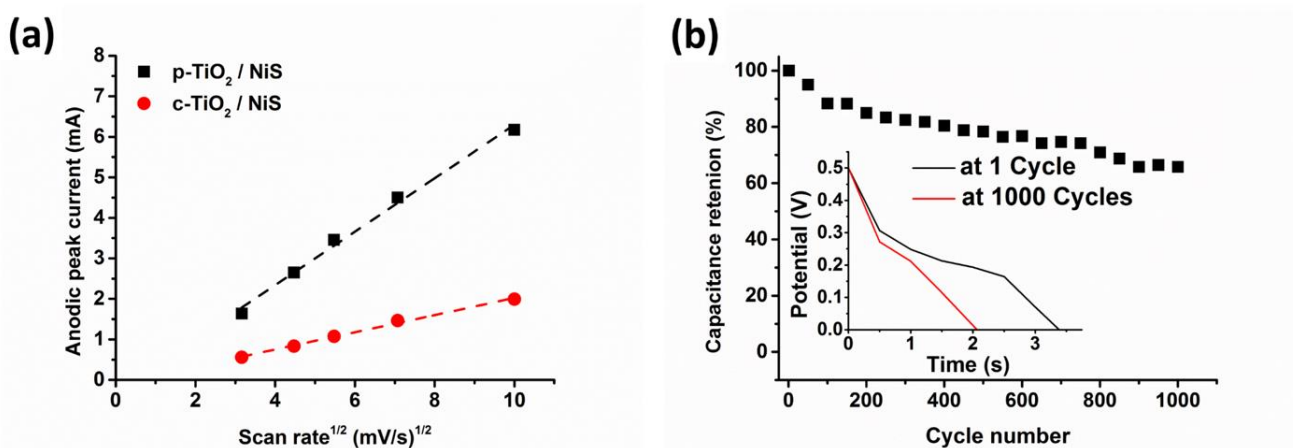


Figure 10. (a) Plots of the anodic peak current as a function of the square root of scan rate of the p-TiO₂/NiS (black) and c-TiO₂/NiS electrodes. The dashed lines are linear fits. (b) Plot of C_{sp} retention for the 7-cycle NiS deposited p-TiO₂/NiS electrode as a function of the number of galvanostatic charge-discharge cycles. (Inset) Galvanostatic charge-discharge curves measured after 1 and 1000 cycles at a constant current density of 3.0 mA/cm².

The almost linear i_p vs. v plots of the p-TiO₂/NiS and c-TiO₂/NiS electrodes shown in Fig. 10(a) represent the pseudocapacitive characteristics of the electrodes. The approximately 3.1 times larger slope for the p-TiO₂/NiS electrode also indicates its significantly larger surface area compared to that of the c-TiO₂/NiS electrode. This is because the n , C_0 and v values were constant, and the D value of the p-TiO₂/NiS electrode is probably not larger than that of the c-TiO₂/NiS electrode since the D value is known to decrease as particle size becomes smaller [41]. The cycle stability of the p-TiO₂/NiS electrode was examined by repeating continuous GCD cycles at a constant current density of 3 mA/cm². Fig. 10(b) represents the C_{sp} retention as a function of the cycle numbers, and the inset shows the galvanostatic curves measured after 1 and 1000 charge-discharge cycles. Similar to previous reports for NiS electrodes [12,13,42], a relatively steeper decrease in the capacitance occurred during the first 100 cycles. This could be attributed to the irreversible reaction between the electrode materials and the electrolyte, including the phase transformation from NiS to Ni(OH)₂ [42,43].

4. CONCLUSION

A nanostructured NiS electrode for supercapacitor applications was prepared by repeated cycles of alternate dip-coating of NiS onto TiO₂ nanoparticles. The thickness of NiS was controlled by the number of alternate dip-coating cycles; each cycle takes only 6 min. A maximum specific capacitance of 1044 F/g at a scan rate of 1 mA/cm² was obtained for the 7 cycle coated p-TiO₂/NiS electrode. In addition to the superior capacitance, the voltammetric response retention at high scan rates for the nanostructured NiS electrode was significantly larger than that for the planar NiS electrode fabricated on compact TiO₂ layer. These enhancements in capacitive properties of the nanostructured electrode were attributed to the increased surface area and effective contact with the

electrolyte. The results presented here demonstrate the benefits of the alternate dip-coating method for fabricating nanostructured NiS electrodes for supercapacitors.

ACKNOWLEDGEMENTS

This work was supported by National Research Foundation of Korea (NRF) Grants (No.2016R1A5A1012966 and NRF-2013R1A1A2A10012336) funded by the Korean Government.

References

1. V. Augustyn, P. Simon, and B. Dunn, *Energy Environ. Sci.*, 7 (2014) 1597.
2. P. Simon and Y. Gogotsi, *Nat. Mater.*, 7 (2008) 845.
3. G.P. Wang, L. Zhang and J.J. Zhang, *Chem. Soc. Rev.*, 41 (2012) 797.
4. L.L. Zhang and X.S. Zhao, *Chem. Soc. Rev.*, 38 (2009) 2520.
5. J. Yan, Q. Wang, T. Wei and Z. Fan, *Adv. Energy Mater.*, 4 (2014) 1300816.
6. X. Rui, H. Tan and Q. Yan, *Nanoscale*, 6 (2014) 9889.
7. L. Hou, C. Yuan, D. Li, L. Yang, L. Shen, F. Zhang and X. Zhang, *Electrochim. Acta*, 56 (2011) 7454.
8. B. Guan, Y. Li, B. Yin, K. Liu, D. Wang, H. Zhang and C. Cheng, *Chem. Eng. J.*, 308 (2017) 1165.
9. K.J. Huang, J.Z. Zhang and Y. Fan, *J. Alloy. Compd.*, 625 (2015) 158.
10. P. Justin and G.R. Rao, *Int. J. Hydrogen Energ.*, 35 (2010) 9709.
11. J. Yan, G. Lui, R. Tjandra, X. Wang, L. Rasenthiram and A. Yu, *RSC Adv.*, 5 (2015) 27940.
12. A. Wang, H. Wang, S. Zhang, C. Mao, J. Song, H. Niu, B. Jin and Y. Tian, *Appl. Surf. Sci.*, 282 (2013) 704.
13. T. Zhu, Z. Wang, S. Ding, J.S. Chen and X.W. Lou, *RSC Adv.*, 1 (2011) 397.
14. J. Yang, X. Duan, W. Guo, D. Li, H. Zhang and W. Zheng, *Nano Energy*, 5 (2014) 74..
15. L. Huang, H.J. Hou, B.C. Liu, K. Zeinu, X.Q. Yuan, X.L. Zhu, X.L. He, L.S. Wu, J.P. Hu and J.K. Yang, *Ceramics Int.*, 43 (2017) 3080.
16. X. Yan, X. Tong, L. Ma, Y. Tian, Y. Cai, C. Gong, M. Zhang, and L. Liang, *Mater. Lett.*, 124 (2014) 133.
17. Z. Li, A. Gu, J. Sun and Q. Zhou, *New J. Chem.*, 40 (2016) 1663.
18. B. You and Y. Sun, *Adv. Energy Mater.*, 6 (2016) 1502333.
19. X. Ma, L. Zhang, G. Xu, C. Zhang, H. Song, Y. He, C. Zhang and D. Jia, *Chem. Eng. J.*, 320 (2017) 22.
20. Y. Xu, W. Du, L. Du, W. Zhu, W. Guo, J. Chang, B. Zhang and D. Deng, *RSC Adv.*, 7 (2017) 22553.
21. F. Cai, R. Sun, Y. Kang, H. Chen, M. Chen and Q. Li, *RSC Adv.*, 5 (2015) 23073.
22. H. Chen, J. Li, C. Long, T. Wei, G. Ning, J. Yan and Z. Fan, *J. Marine Sci. Appl.*, 13 (2014) 462.
23. L. Zuo, W. Fan, Y. Zhang, Y. Huang, W. Gai and T. Liu, *Nanoscale*, 9 (2017) 4445.
24. R. Liu, J. Duay and S.B. Lee, *Chem. Commun.*, 47, (2011) 1384.
25. J. Duay, S.A. Sherrill, Z. Hui, E. Gillette and S.B. Lee, *Acs Nano*, 7 (2013) 1200.
26. I. Ryu, G. Kim, D. Park and S. Yim, *J. Power Sources*, 297 (2015) 98.
27. X. Lu, G. Wang, T. Zhai, M. Yu, J. Gan, Y. Tong and Y. Li, *Nano Lett.*, 12 (2012) 1690.
28. X. Lu, M. Yu, G. Wang, T. Zhai, S. Xie, Y. Ling, Y. Tong and Y. Li, *Adv. Mater.*, 25 (2013) 267.
29. G. Wang, H. Wang, Y. Ling, Y. Tang, X. Yang, R. C. Fitzmorris, C. Wang, J. Z. Zhang and Y. Li, *Nano Lett.*, 11 (2011) 3026.
30. S.D. Mo and W.Y. Ching, *Phys. Rev. B*, 51 (1995) 13023.
31. B. Oregon and M. Gratzel, *Nature*, 353 (1991) 737.

32. C. Sun, M. Ma, J. Yang, Y. Zhang, P. Chen, W. Huang, and X. Dong, *Sci Rep.*, 4 (2014) 7054.
33. R. Liu, J. Duay, and S. Lee, *Chem. Commun.*, 47 (2011) 1384.
34. X. Xia, J. Tu, Y. Zhang, X. Wang, C. Gu, X. Zhao, and H. J. Fan, *ACS Nano*, 6 (2012) 5531.
35. Y. Li, B. Tan, and Y. Wu, *J. Am. Chem. Soc.*, 128 (2006) 14258.
36. J. Li, E. Shangguan, D. Guo, M. Tian, Y. Wang, Q. Li, Z. Chang, X. Zi. Yuan and H. Wang, *J. Power Sources*, 270 (2014) 121.
37. I.E. Rauda, V. Augustyn, B. Dunn and S.H. Tolbert, *Acc. Chem. Res.*, 46 (2013) 1113.
38. H. Kwon, D. Hong, I. Ryu and S. Yim, *ACS Appl. Mater. Interf.*, 9 (2017) 7412.
39. E. Shangguan, Z. Chang, H. Tang, X. Zi. Yuan and H. Wang, *J. Power Sources*, 196 (2011) 7797.
40. L. Lei, M. Hu, X. Gao and Y. Sun, *Electrochim. Acta*, 54 (2008) 671.
41. J. Wang, J. Polleux, J. Lim and B. Dunn, *J. Phys. Chem. C*, 111 (2007) 14925.
42. J. Yang, X. Duan, Q. Qin and W. Zheng, *J. Mater. Chem. A*, 1 (2013) 7880.
43. Y. Xiao, S. Liu, F. Li, A. Zhang, J. Zhao, S. Fang and D. Jia, *Adv. Funct. Mater.*, 22 (2012) 4052.

© 2017 The Authors. Published by ESG (www.electrochemsci.org). This article is an open access article distributed under the terms and conditions of the Creative Commons Attribution license (<http://creativecommons.org/licenses/by/4.0/>).